Decoupling Registration from Measurement: Longitudinal 3D Wound Assessment Anchored to Stable Peri-Wound Skin

Chengtao Ma[1], **Haidong Yang**[1]
[1]School of Information Engineering, Inner Mongolia University of Technology, Hohhot, Inner Mongolia 010080, China
Corresponding author: Haidong Yang (e-mail: imperman@imut.edu.cn).

ABSTRACT Longitudinal three-dimensional wound assessment requires stable spatial correspondences across scans, yet the wound surface–the very region to be measured–changes continuously through contraction, granulation, and remodelling. Including it in registration risks absorbing genuine healing change into the spatial transformation, biasing longitudinal measurements. We decouple registration from measurement by anchoring alignment exclusively to the peri-wound healthy skin while excluding the wound from correspondence construction and transform fitting. A coarse-to-fine rigid-registration pipeline, enhanced by wound-edge distance-decaying weighting, selects the best transformation automatically from multiple candidates. On seven longitudinal tasks across four chronic-wound cases referenced to the first scan, the method achieved mean fitness of 0.57 $\pm$ 0.27, root-mean-square error (RMSE) of 2.44 $\pm$ 0.94 mm, and overlap ratio of 57.98 $\pm$ 22.68%. Where both conventional baselines failed completely, the method still produced usable alignments (fitness $>$ 0.10, overlap $>$ 15%). Spatial weighting further reduced mean RMSE to 2.15 mm, enabling unified quantification of wound area, volume, and depth. These findings indicate that a stable anatomical reference may matter more than algorithmic complexity in longitudinal lesion tracking–a decoupling principle applicable beyond wound care.

INDEX TERMS Chronic wound, dynamic quantitative evaluation, healthy-skin anchor, point cloud registration, three-dimensional longitudinal registration

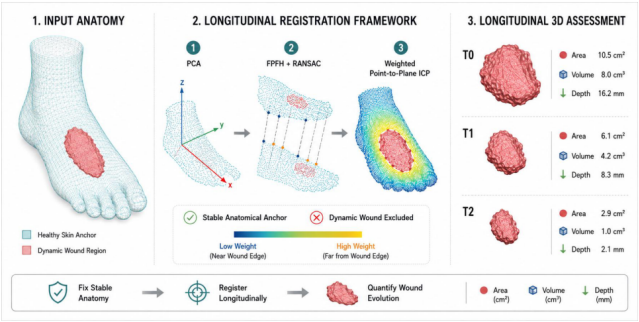

I. INTRODUCTION

THIS section introduces the clinical motivation, the unresolved challenge of longitudinal wound registration, and the core idea of anchoring spatial alignment to stable peri-wound healthy skin.

A. RESEARCH BACKGROUND

Chronic wounds are characterised by prolonged healing, high recurrence, and frequent complications, and they remain a persistent burden on healthcare resources [1]. Pressure injuries, venous leg ulcers, and diabetic foot ulcers are among the most representative clinical forms, often leading to infection, amputation, and substantial quality-of-life loss [2], [3]. Timely treatment adjustment therefore depends on continuous, objective, and accurate assessment of healing.

Yet routine clinical evaluation still relies heavily on contact tools such as rulers and probes, which carry a risk of cross-infection and cannot reproduce wound geometry faithfully [4]. Even common non-contact area surrogates such as the longest-length by widest-width estimate systematically overestimate irregular wounds [5]. Manual two-dimensional records also fail to capture the three-dimensional remodelling that defines long-term healing [6]. Better quantitative follow-up tools are therefore urgently needed.

Three-dimensional imaging now makes non-contact and repeatable wound assessment technically feasible, but reliable longitudinal follow-up remains unresolved. Structured-light scanners, RGB-D devices, and smartphone photogrammetry can reconstruct wound geometry with increasing precision and accessibility [7]-[10]. In parallel, recent segmentation methods, including deep-learning and foundation-

model-based approaches, have improved wound-boundary extraction and automated quantification [11]-[16]. Together, these advances have made single-scan 3D wound assessment increasingly practical in clinical workflows.

However, the main clinical question is not how a wound looks at one visit, but how it changes across weeks or months. Longitudinal analysis requires stable spatial correspondences across time points, while the wound itself contracts, remodels, and changes topologically during healing [17], [18]. If the wound surface is used as the registration reference, part of the true biological change can be absorbed into the transformation itself, biasing downstream measurements.

This problem creates a methodological paradox: to measure healing we must align scans across time, yet the most salient geometric structure–the wound surface itself–is exactly what is changing. For example, if wound contraction reduces the area by 30% between visits, a registration that includes the wound surface may partially undo that contraction during alignment, thereby underestimating the true longitudinal change.

We address this gap by anchoring registration exclusively to the peri-wound healthy-skin anchor and treating the wound only as the measurement target. This separation preserves a stable coordinate system, reduces the risk of absorbing genuine tissue change into the rigid transformation, and provides the conceptual basis for the method developed in this paper.

B. RELATED WORK

Establishing stable longitudinal correspondence remains challenging because both anatomy and acquisition conditions vary across visits. Healing introduces centripetal contraction, granulation tissue formation, and re-epithelialisation-driven remodelling [18], while posture variation, skin elasticity, and acquisition noise further enlarge the discrepancy between time points. Registration methods designed for static targets are therefore only partially suitable for chronic-wound follow-up.

Existing registration research mainly addresses how to align point clouds more robustly. Iterative closest point (ICP) and its point-to-plane variant remain standard tools for fine alignment [19], [20], whereas RANSAC and FPFH support coarse registration under noise and partial overlap [21], [22]. Statistical methods such as CPD and Gaussian-mixture-model approaches broaden the modelling perspective, but they do not by themselves determine which anatomical structure should serve as the medically meaningful reference [23], [24].

Clinical-registration studies further show that anatomical priors matter. In surgical navigation and partial-observation settings, registration strategies are often redesigned around incomplete exposure and structural heterogeneity rather than around ideal global overlap [25]. This lesson is directly relevant to chronic wounds, where only part of the surrounding anatomy remains sufficiently stable across visits.

Longitudinal medical-image analysis makes the central risk even clearer: the key issue is not only whether two observations can be aligned, but whether the registration framework absorbs true pathological change. Work on unbiased within-subject templates, non-uniform appearance change, and registration-based change tracking repeatedly shows that, without explicit constraints on what should remain invariant, registration may suppress clinically meaningful evolution instead of preserving it [26]-[35].

Existing longitudinal wound studies generally either include the whole wound region in alignment or rely on increasingly complex deformation models to fit cross-time-point differences. We instead ask a prior question: which anatomical region should define the spatial reference in the first place? Our answer is that reference definition comes before algorithmic complexity: without a stable reference, a more sophisticated registration model can still produce a less interpretable longitudinal measurement.

C. CONTRIBUTIONS AND PAPER ORGANISATION

Motivated by this gap, we propose a longitudinal registration framework for chronic wounds that separates the spatial reference from the dynamic measurement target. The method uses peri-wound healthy skin as the only registration anchor and excludes the dynamic wound region from direct correspondence construction and rigid-transform estimation. The main contributions are as follows.

(1) *Reference definition.* We define peri-wound healthy skin as the sole registration anchor, while treating the dynamic wound region only as the downstream measurement target. This design preserves the interpretability of longitudinal morphological comparison.

(2) *Registration pipeline.* We build a three-stage pipeline consisting of PCA pre-alignment, multi-candidate RANSAC coarse registration, and ICP refinement, with automatic candidate selection to improve robustness under long-term follow-up.

(3) *Spatial prior enhancement.* We introduce a wound-edge-distance-based spatial weighting strategy so that stable healthy-skin regions farther from the wound edge contribute more strongly during refinement, improving local alignment precision without changing the overall framework.

Taken together, these contributions show that a medically rational reference definition can make classical rigid registration more stable and interpretable in realistic longitudinal wound assessment.

This central claim guides the rest of the paper. Section II presents data acquisition, region definition, segmentation, registration, and quantification. Section III reports the main registration, ablation, and quantification results. Section IV interprets these findings, discusses method boundaries, and analyses limitations and future directions. Section V summarises the main conclusion.

II. MATERIALS AND METHODS

A. DATA ACQUISITION AND REGION DEFINITION

We first describe the data foundation of the study and why the resulting longitudinal measurements remain comparable across follow-ups. We acquired coloured 3D point clouds of chronic wounds using a Shining 3D EinScan-E10 hand-held structured-light scanner. The device captures both wound geometry and natural texture through binocular structured-light imaging. To ensure comparability across time points, we standardised scanning distance, acquisition range, and reconstruction density across all subjects.

All subjects underwent multi-time-point follow-up under a unified protocol. Before scanning, we cleaned the wound, removed dressings, and fully exposed at least 5 cm of surrounding skin. During acquisition, we kept body position, scanning angle, and device distance as consistent as possible to reduce systematic error from posture variation. The first acquisition is denoted T0, and subsequent follow-ups are denoted T1 and T2.

For region definition, the local point cloud at each time point is divided into the following three functional regions:
1) *Full local anatomical region (full region of interest, ROI):* contains the wound and the surrounding local limb tissue, preserving the overall anatomical context.
2) *Peri-wound healthy-skin anchor:* defined as the skin region within a certain distance from the wound edge that shows no obvious scar traction, no exudate coverage, and no tissue defect. This region serves as the sole spatial registration reference.
3) *Dynamic wound region (wound region):* contains the wound itself and the adjacent dynamic area; it is used for area, volume and depth analysis after spatial unification and is excluded from direct correspondence construction and rigid-transform fitting during registration.

This partitioning decouples the spatial reference from the dynamic measurement target.

B. WOUND REGION SEGMENTATION AND 3D POINT CLOUD MAPPING

We next describe how we separate the healthy-skin anchor from the dynamic wound region and propagate the two-dimensional segmentation result back to the three-dimensional point cloud. To do so, we construct an interactive segmentation pipeline based on the Segment Anything Model (SAM).

Bed sheets, clothing and other background structures are common occluders in the clinical acquisition setting; running wound segmentation directly on the texture image readily introduces false positives. A two-stage "body first, wound second" strategy is therefore adopted. In the first stage, the operator draws a bounding box around the whole limb region on the texture image, and SAM outputs the body mask to remove the background and produces the corresponding body point cloud. In the second stage, each wound is enclosed in its own bounding box within the body region, SAM returns candidate wound masks, and the boundaries are locally refined through foreground/background point interaction.

After 2D segmentation, the structured-light projection model links the texture image to the 3D point cloud. Points whose projected coordinates fall inside the wound mask are classified as wound points; points inside the body region but outside the wound mask are classified as healthy-skin-anchor points; and points outside the body region are treated as background and discarded. This process yields three point-cloud classes–full ROI, healthy-skin anchor, and wound–which provide a unified data source for downstream longitudinal registration and quantification.

C. LONGITUDINAL RIGID REGISTRATION ALGORITHM

We summarise the proposed longitudinal rigid-registration pipeline in Algorithm 1. The pseudocode emphasises the data flow and decision logic rather than low-level implementation details.

Algorithm 1 Pseudocode of the healthy-skin-anchor-based longitudinal rigid registration pipeline

1: Input: reference scan P_{ref}, follow-up scan P_{mov}, healthy-skin-anchor masks, wound mask, registration parameters
2: Initialization: extract healthy-skin-anchor point clouds from P_{ref} and P_{mov}; set candidate set $C \leftarrow \varnothing$
3: Perform PCA-based pose pre-alignment
4: Enumerate axis-polarity combinations and select the initial pose by maximum anchor overlap
5: If rotation angle > 80 degree, apply translation reset
6: Downsample anchor point clouds with a 5 mm voxel grid
7: Compute FPFH descriptors and run RANSAC coarse registration
8: Run point-to-plane ICP refinement
9: If spatial weighting is enabled, compute distance from each anchor point to the wound or scar set W, assign an exponential spatial-prior weight, combine it with a Tukey residual weight, and solve a weighted least-squares ICP update
10: Retain candidate transformations: PCA pre-alignment, RANSAC coarse registration, ICP from PCA, ICP from RANSAC
11: Select final transformation T^* by lexicographic ranking using overlap ratio, fitness, and RMSE
Output: final rigid transformation T^*, registered wound point cloud, registration metrics

Algorithm 1 reorganises the registration workflow into initialization, coarse-to-fine rigid fitting, an optional spatial-weighting branch, and lexicographic candidate selection. The dynamic wound region is excluded from direct correspondence construction and rigid-transform fitting, while the healthy-skin anchor defines the stable spatial reference.

D. LONGITUDINAL WOUND QUANTIFICATION

Before downstream measurement, we assess whether the longitudinal alignment is sufficiently stable to support quantitative analysis. We use four metrics to characterise registration quality on the healthy-skin-anchor region: fitness, which reflects the proportion of valid corresponding points; root-mean-square error (RMSE), which quantifies the mean spatial error of corresponding points; overlap ratio, which assesses spatial overlap in the unified coordinate system; and rotation angle, which reports the magnitude of the final rigid transformation and helps analyse the effect of pose variation on registration stability.

Once the registration is judged stable, the wound region at each time point is mapped to the unified anatomical coordinate system. We then compute area, volume, maximum depth, and mean depth to characterise spatial morphological change throughout healing. Together, these 3D indices provide a longitudinal description of wound evolution.

E. STUDY SUBJECTS AND ETHICAL APPROVAL

This study is a prospective clinical observational study, conducted in May 2026 at the Department of Burn Surgery, Inner Mongolia Baogang Hospital. The study protocol was approved by the Medical Ethics Committee of Inner Mongolia Baogang Hospital prior to data acquisition (approval number: 2026-MER-024), and all study procedures strictly conformed to the Declaration of Helsinki (2013 revision).

Inclusion criteria were: patients aged 18 to 70 years; meeting the clinical diagnostic criteria for chronic wounds; able to complete at least two follow-up scans; presence of a relatively stable healthy-skin region around the wound suitable for registration; and voluntary signing of informed consent. Subject data were anonymised, and only a study identifier was retained for subsequent analysis.

III. RESULTS

A. DATASET AND EXPERIMENTAL SETUP

Four chronic-wound cases define the experimental setting used throughout the Results. Case_1, Case_2, and Case_3 each include three time points (T0, T1, T2), whereas Case_4 includes T0 and T1 only, yielding 7 longitudinal registration tasks referenced to T0. All cases were acquired with the same scanner, processed with the same segmentation pipeline, and registered with the same parameter set, enabling a controlled comparison across follow-up lengths.

Two classical rigid-registration methods were used as baselines: traditional point-to-point ICP and point-to-plane ICP with a robust constraint. The proposed method follows a "PCA pre-alignment–RANSAC coarse registration–point-to-plane ICP refinement" pipeline, and uses only the healthy-skin-anchor point cloud for the final transformation estimation. The evaluation metrics include fitness, root-mean-square error (RMSE), overlap ratio and rotation angle.

B. OVERALL REGISTRATION PERFORMANCE OF DIFFERENT METHODS

The proposed method performs clearly better than point-to-point ICP and remains close overall to the robust point-to-plane baseline. Table I summarises the overall results across all seven longitudinal registration tasks, with mean fitness, RMSE, and overlap ratios of 0.50 ± 0.25, 2.59 ± 0.38 mm, and $50.45\% \pm 18.94\%$ for point-to-point ICP; 0.58 ± 0.29, 1.85 ± 0.31 mm, and $58.25\% \pm 27.39\%$ for robust point-to-plane ICP; and 0.57 ± 0.27, 2.44 ± 0.94 mm, and $57.98\% \pm 22.68\%$ for the proposed method. The current sample of four chronic-wound cases remains relatively limited for drawing definitive conclusions regarding statistical superiority, but it

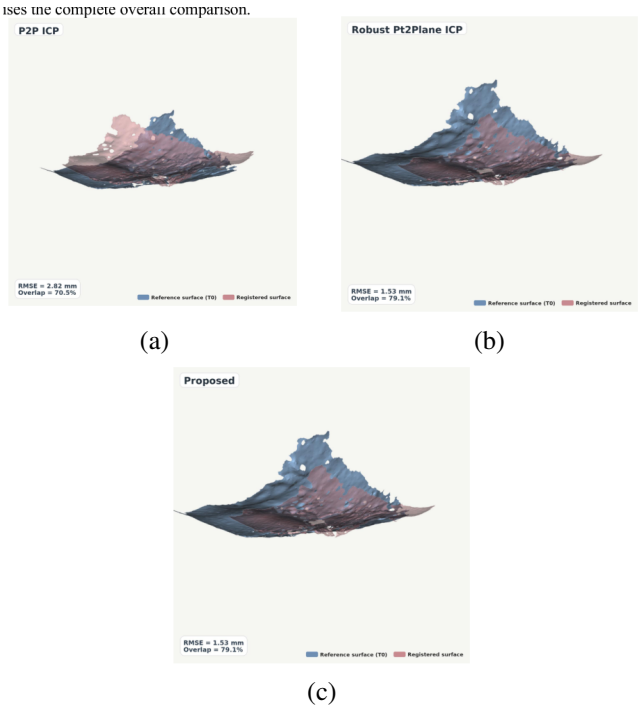

FIGURE 1. Representative registration performance comparison for Case_2/T2. (a) Point-to-point ICP. (b) Robust point-to-plane ICP. (c) Proposed healthy-skin-anchor method. Blue indicates the reference surface at T0, and pink indicates the registered follow-up surface. RMSE is reported in mm and overlap is reported as a percentage. All panels were uniformly cropped from full-frame renderings and resized without local contrast or brightness adjustment.

provides a meaningful basis for comparing methodological behaviour.

Case-level differences are more informative. The examples below highlight typical convergence behaviour, near-equivalent performance between methods, and situations in which the healthy-skin-anchor strategy shows practical value across the four study cases.

On Case_1/T1 and Case_3/T1, the proposed method converges to exactly the same final result as robust point-to-plane ICP. On Case_1/T2, Case_2/T2, and Case_3/T2, the two methods are also nearly identical in fitness, RMSE, and overlap ratio. The most informative difficult example is Case_4/T1, where the robust baseline fails completely (fitness = 0, RMSE = inf) but the proposed method still produces a usable result (fitness = 0.1037, RMSE = 3.8345 mm, overlap = 15.46%). By contrast, Case_2/T1 shows that performance can still degrade when healthy-skin-anchor coverage changes markedly in spatial distribution. Fig. 1 presents one representative visual example, and Table I summarises the complete overall comparison.

C. SPATIALLY WEIGHTED ICP ENHANCEMENT EXPERIMENT

Spatial weighting reduces local registration error without changing the global ranking of candidate transformations. To test whether the wound-edge distance prior improves alignment on the healthy-skin-anchor region, we add spa-

TABLE 1. Overall registration performance of different methods (mean ± SD).

Method	Fitness	RMSE (mm)	Overlap Ratio (%)	Rotation (deg)
point-to-point ICP	0.50±0.25	2.59±0.38	50.45±18.94	18.02±27.69
Robust point-to-plane ICP	0.58±0.29	1.85±0.31	58.25±27.39	14.44±8.18
Proposed Method	0.57±0.27	2.44±0.94	57.98±22.68	23.22±19.17

Note: fitness denotes the inlier correspondence ratio; RMSE is reported in mm; overlap ratio is reported as a percentage; rotation is reported in degrees; SD, standard deviation.

tially weighted point-to-plane ICP to the original three-stage pipeline and perform a six-group parameter sweep over spatial_weight_min, spatial_weight_sigma_quantile, and spatial_weight_power. The best configuration, group D (0.4, 0.5, 1.0), lowers the mean RMSE from 2.44 mm to 2.15 mm, a reduction of 0.29 mm (12.0%). However, this RMSE improvement comes at the cost of a marginal decrease in mean fitness from 0.5694 to 0.5659 and in mean overlap ratio from 57.98% to 57.43%. Spatial weighting therefore improves local geometric consistency more than overall correspondence coverage.

The benefit of spatial weighting is selective rather than uniform across difficult cases. On Case_2/T1, the final metrics of the original and weighted methods are identical (fitness = 0.3960, RMSE = 3.6820 mm, overlap = 45.30%), indicating that once coarse registration has already deviated from the correct correspondence, reweighting within ICP alone cannot recover the global mismatch. On the more difficult Case_4/T1, spatial weighting raises fitness from 0.1037 to 0.1151, reduces RMSE from 3.8345 mm to 2.0750 mm, and increases overlap ratio from 15.46% to 18.14%, demonstrating a meaningful local-correction effect. Across the current dataset, the chosen-transform breakdown indicates that group D most often preserves or strengthens the ICP refinement stage, while in difficult mismatched cases it may still retain an earlier candidate such as the PCA result for Case_2/T1. This pattern indicates that spatial weighting mainly strengthens the refinement stage.

D. EFFECT OF THE REGISTRATION REFERENCE ON PERFORMANCE (ABLATION STUDY)

Healthy-skin-anchor registration preserves measurement interpretability at only a marginal cost in average numerical metrics. Table II shows that the full ROI input yields mean fitness, RMSE, and overlap ratio of 0.58 ± 0.26, 2.06 ± 0.84 mm, and 58.87% ± 20.95%, whereas the healthy-skin-anchor input yields 0.57 ± 0.27, 2.44 ± 0.94 mm, and 57.98% ± 22.68%. These differences remain small on the current sample and do not establish a decisive statistical advantage for either setting.

The key issue is interpretability rather than a marginal gain in average metrics. When the full ROI is used for registration, the dynamic wound region simultaneously serves as the alignment reference and the measurement target. Under that design, part of the true biological change can

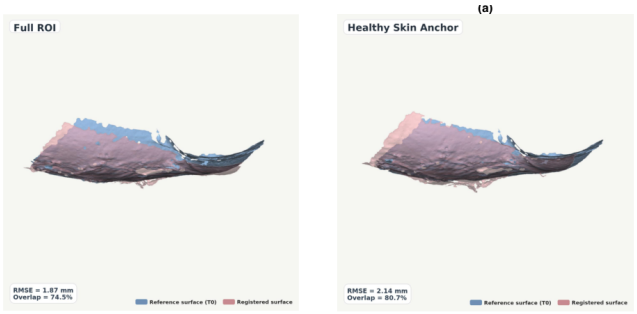

(a) (b)

FIGURE 2. Representative comparison of registration reference definitions for Case_1/T2. (a) Registration using the full ROI point cloud. (b) Registration using only the healthy skin anchor region. Blue indicates the reference surface at T0, and pink indicates the registered follow-up surface. RMSE is reported in mm and overlap is reported as a percentage. All panels were uniformly cropped from full-frame renderings and resized without local contrast or brightness adjustment.

TABLE 2. Effect of different registration references on performance (mean ± SD).

Registration Input	Fitness	RMSE (mm)	Overlap Ratio (%)
Full ROI Point Cloud	0.58±0.26	2.06±0.84	58.87±20.95
Healthy Skin Point Cloud	0.57±0.27	2.44±0.94	57.98±22.68

Note: full ROI indicates the complete region-of-interest point cloud; RMSE is reported in mm; overlap ratio is reported as a percentage; SD, standard deviation.

be absorbed into the spatial transformation itself, which may lower numerical error by partially registering away the very contraction or remodelling that should be measured. The healthy-skin anchor avoids this conceptual confound and therefore remains the more defensible reference for longitudinal medical measurement. See Table II and Fig. 2 for details.

E. CONTRIBUTION ANALYSIS OF THE THREE-STAGE REGISTRATION PIPELINE

Each stage of the three-stage pipeline contributes progressively to the final convergence. Table III shows the performance evolution from the raw point cloud through PCA pre-alignment, RANSAC coarse registration, and ICP refinement. At the raw stage, the mean fitness is only 0.04 ± 0.08 and the mean RMSE is 3.78 ± 0.15 mm, confirming that the original coordinates alone rarely support stable cross-time-point correspondence. PCA pre-alignment raises mean fitness to 0.44 ± 0.28 and reduces mean RMSE to 3.52 ± 0.38 mm, showing the value of principal-axis normalisation for correcting initial pose deviation. RANSAC coarse registration further improves mean fitness to 0.45 ± 0.27 and mean RMSE to 3.32 ± 0.46 mm. ICP refinement then raises mean fitness to 0.57 ± 0.27 and lowers mean RMSE to 2.44 ± 0.94 mm, confirming that local refinement remains indispensable.

The final performance arises from the progressive synergy of the whole pipeline rather than from any single module.

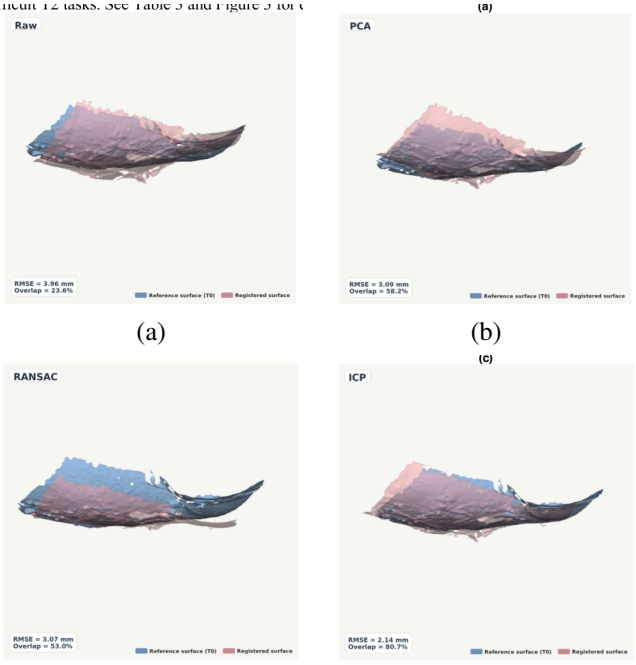

FIGURE 3. Representative stage-wise registration results for Case_1/T2. (a) Raw point cloud. (b) PCA pre-alignment. (c) RANSAC coarse registration. (d) ICP refinement. Blue indicates the reference surface at T0, and pink indicates the registered follow-up surface. RMSE is reported in mm and overlap is reported as a percentage. All panels were uniformly cropped from full-frame renderings and resized without local contrast or brightness adjustment.

TABLE 3. Performance changes across the multi-stage registration pipeline (mean ± SD).

Stage	Fitness	RMSE (mm)
Raw Point Cloud	0.04±0.08	3.78±0.15
PCA Pre-alignment	0.44±0.28	3.52±0.38
RANSAC Coarse Registration	0.45±0.27	3.32±0.46
ICP Refinement	0.57±0.27	2.44±0.94

Note: RMSE is reported in mm; fitness denotes the inlier correspondence ratio; SD, standard deviation.

PCA provides a stable initialisation, RANSAC supplies coarse global correspondence, and ICP performs the final local refinement. This staged effect is even more evident on the more difficult T2 tasks. See Table III and Fig. 3 for details.

F. THREE-DIMENSIONAL WOUND QUANTIFICATION RESULTS

Representative case-level longitudinal 3D quantification reveals wound changes that a single two-dimensional metric cannot capture. To illustrate typical healing trajectories within the four study cases, Table IV reports representative longitudinal quantification results from all four included cases.

Case_1 shows clear early healing, with area and volume at T1 decreasing by 57.48% and 96.55% relative to T0; at T2, the area rises slightly by 7.02% relative to T0 while volume still decreases by 60.51%, suggesting late remodelling with

TABLE 4. Representative longitudinal 3D wound quantification results.

Case	Time Point	Area (cm^2)	Volume (cm^3)	Maximum Depth (mm)	Mean Depth (mm)	Area Change (%)	Volume Change (%)
Case_1	T0	10.48	8.04	16.24	6.93	0.00	0.00
Case_1	T1	4.45	0.28	2.78	0.52	-57.48	-96.55
Case_1	T2	11.21	3.18	9.74	2.76	7.02	-60.51
Case_2	T0	43.95	15.58	11.76	3.35	0.00	0.00
Case_2	T1	51.03	36.43	12.38	7.35	16.11	133.83
Case_2	T2	55.38	38.81	13.64	7.40	26.00	149.10
Case_3	T0	0.95	0.16	2.44	1.67	0.00	0.00
Case_3	T1	0.50	0.10	3.57	2.01	-47.06	-37.09
Case_3	T2	0.76	0.17	3.12	2.27	-19.20	3.91
Case_4	T0	96.26	118.48	21.77	12.20	0.00	0.00
Case_4	T1	184.66	101.63	24.27	6.44	91.83	-14.22

Note: area is reported in cm^2; volume is reported in cm^3; maximum depth and mean depth are reported in mm; percentage changes are relative to T0 within each case.

shallowing despite local surface expansion. Case_2 shows continuous worsening, with both area and volume increasing at T1 and T2 and volume at T2 rising by 149.10% relative to T0. Case_3 shows only mild fluctuation, whereas Case_4 combines marked area expansion with reduced mean depth. Together, these representative patterns show that area, volume, and depth evolve asynchronously and should be interpreted jointly.

Given stable registration, representative longitudinal 3D quantification provides more than a coarse judgement of healing versus non-healing. It reveals asynchronous trajectories across area, volume, and depth and therefore offers a more objective basis for analysing remodelling pathways and treatment differences in chronic wounds, while the full dataset-level registration performance is summarised separately in the preceding sections. See Table IV for representative case details.

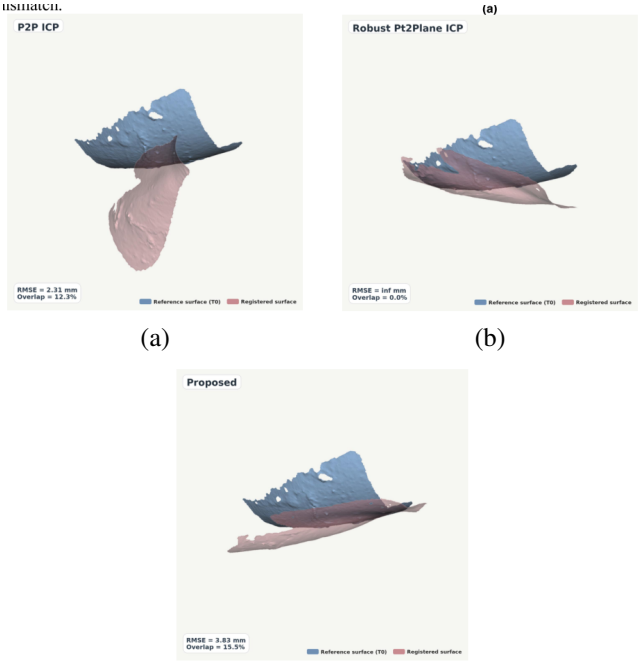

FIGURE 4. Representative registration outcome for the difficult case Case_4/T1. (a) Point-to-point ICP. (b) Robust point-to-plane ICP. (c) Proposed healthy-skin-anchor method. Blue indicates the reference surface at T0, and pink indicates the registered follow-up surface. RMSE is reported in mm and overlap is reported as a percentage. All panels were uniformly cropped from full-frame renderings and resized without local contrast or brightness adjustment.

IV. DISCUSSION

A. PRINCIPAL FINDINGS

The central finding of this study is that, in longitudinal wound follow-up, choosing the correct spatial reference is more important than simply pursuing a more complex registration model. Rather than treating registration accuracy as a purely numerical optimisation problem, we argue that longitudinal measurement must first be grounded in a stable and repeatable anatomical basis. This is why the method anchors alignment to the peri-wound healthy-skin anchor instead of fitting the changing wound directly.

On seven longitudinal registration tasks from four chronic-wound cases, the proposed method outperforms traditional point-to-point ICP overall and remains close to the robust point-to-plane baseline. Stage-wise analysis further shows that PCA, RANSAC, and ICP each contribute positively to final convergence. Within the four study cases, Case_4/T1 is especially informative: the robust baseline fails completely, whereas the proposed method still returns a usable result. A representative visual comparison for this difficult case is shown in Fig. 4. By contrast, the weaker result on Case_2/T1 shows that the method does not remove instability when healthy-skin-anchor coverage changes markedly.

The spatial-weighting experiment further indicates that wound-edge distance priors can reduce local error without changing the broader behaviour of the pipeline: the optimal configuration D lowers mean RMSE from 2.44 mm to 2.15 mm and reduces the RMSE on Case_4/T1 from 3.83 mm to 2.08 mm, but neither fitness nor overlap improves accordingly. Spatial weighting is therefore best understood as a fine-refinement enhancement rather than a solution to global mismatch.

B. RATIONALE FOR USING STABLE ANATOMY AS THE REGISTRATION REFERENCE

Using stable anatomy as the registration reference is methodologically necessary because the wound itself is the structure that changes. Many longitudinal wound-registration approaches assume that incorporating as much surface information as possible should improve alignment and therefore include the full wound region in transformation estimation. However, chronic wounds undergo contraction, hyperplasia, epithelialisation, and scar remodelling throughout healing. If the changing lesion is also used as the registration reference, the measurement framework becomes self-confounded and introduces systematic bias.

For this reason, we use the peri-wound healthy-skin anchor as the registration reference. Although the present ablation study does not show that healthy-skin-anchor input dominates full-ROI input numerically on average, it remains superior in medical interpretability. The design clearly separates the registration reference from the measurement target and reduces the risk that true tissue change is absorbed into the rigid transformation. In that sense, the primary value of the healthy-skin anchor lies in measurement validity, with numerical performance as a secondary consideration.

C. EFFECTIVENESS AND APPLICABLE BOUNDARY OF THE THREE-STAGE RIGID REGISTRATION

The three-stage rigid-registration pipeline is effective because it addresses instability at progressively finer spatial scales. PCA pre-alignment reduces gross pose discrepancy, RANSAC coarse registration establishes a plausible global correspondence, and ICP refinement provides the local geometric precision required for final alignment. The largest fitness gain occurs between the raw point cloud and PCA, highlighting the importance of correcting posture and principal-axis differences early. ICP then contributes most strongly to the final precision once a reasonable initialisation has been established.

This pipeline also has a clear applicability boundary. It assumes that a sufficiently large and well-distributed healthy-skin anchor remains visible across time points. When anchor coverage is sparse, spatial distribution shifts markedly, or patient pose changes substantially, the method can still fall into incorrect correspondences; Case_2/T1 is an example. Conversely, on extreme cases such as Case_4/T1, the candidate-transformation fallback and automatic selection mechanism help the method avoid complete failure even when the final result is not ideal.

D. SIGNIFICANCE AND BOUNDARY OF THE SPATIAL WEIGHTING ENHANCEMENT

Spatial weighting improves local precision, but its benefit is bounded by the quality of the upstream alignment. The wound-edge distance-decaying prior lowers the mean RMSE to 2.15 mm and markedly reduces error on Case_4/T1. However, fitness and overlap ratio do not improve in parallel, indicating that the strategy mainly stabilises correspondence within the existing anchor region rather than enlarging the valid matching range. Spatially weighted ICP therefore functions best as a refinement enhancement, not as an independent global registration mechanism.

The contrast between Case_2/T1 and Case_4/T1 further shows that spatial weighting is sensitive to the source of mismatch. When coarse registration is already globally incorrect, adjusting point weights within ICP is usually insufficient to recover the right solution. When coarse alignment is essentially correct but local correspondence remains unstable, the spatial prior offers a more meaningful correction. The current results therefore support using spatial weighting as an enhancement module within the original three-stage pipeline.

This judgement is consistent with the consensus on "unbiased registration" in longitudinal medical-image analysis. Both within-subject template estimation and non-uniform intensity-change modelling indicate that, if the registration framework lacks an explicit constraint on which changes belong to real pathological evolution, the algorithm may absorb these changes into the common reference space through deformation or re-correspondence [31], [32]. Chronic wounds are no exception: directly treating the dynamic wound edge in contraction, hyperplasia and epithelialisation as the object to be aligned can yield numerically smoother registration that does not necessarily reflect a more faithful longitudinal measurement. A recent systematic review of registration-based change tracking in radiological imaging also emphasises that registration design in change-tracking tasks should serve lesion fidelity rather than simply maximising geometric overlap [33]. Selecting the stable healthy skin as the unique spatial anchor is in essence a longitudinal-bias-control measurement strategy.

E. POTENTIAL RELATION BETWEEN REGISTRATION ERROR AND TISSUE REMODELLING

Registration error may itself contain information about tissue remodelling, but the current data support this idea only as a hypothesis. We originally asked whether rigid-registration error would vary systematically with the degree of biological remodelling during long-term follow-up. The present cases suggest such a tendency in some instances, but not a strictly monotonic pattern across all subjects. A cautious interpretation is that longer follow-up intervals, stronger wound-edge contraction, and greater scar traction may weaken spatial correspondence over the healthy-skin anchor and thereby increase the difficulty of rigid registration. If confirmed in larger cohorts, this error variation may carry biomechanical meaning and may even become a secondary marker of tissue remodelling.

At present, the data are better suited to hypothesis generation than to clinical conclusion. Longer multi-time-point follow-up combined with scar scores, healing rates, and clinical photographic assessment will be needed to determine whether degradation in registration quality can serve as an indirect indicator of tissue remodelling. This possibility opens a forward-looking question: registration residuals may eventually prove informative not only as technical errors, but also as signals of biologically meaningful remodelling dynamics.

F. LIMITATIONS AND FUTURE WORK

The main limitation of this study is not whether the method can run, but whether the current evidence is sufficient for stable clinical deployment. First, the sample size remains modest: four cases and seven registration tasks provide only limited statistical power for drawing definitive conclusions. Second, the final result depends heavily on the quality and spatial distribution of the healthy-skin anchor, so unstable anchor extraction directly degrades registration. Third, the current framework is rigid; in cases with substantial local traction, elastic deformation, or large pose variation, a purely rigid model may not fully describe real change. Fourth, although the method is more defensible from the perspective of measurement logic, its average numerical performance does not yet establish a clear advantage over the robust baseline. The present contribution is therefore better understood as a medically interpretable registration paradigm than as a claim of uniform numerical superiority.

Future work should proceed in four directions: expanding the case set and follow-up period to test whether the observed error-variation trend has stable clinical significance; improving healthy-skin-anchor extraction under large pose variation and uneven coverage; combining rigid registration with constrained local non-rigid analysis to improve applicability in complex scenarios; and packaging the pipeline into a standardised analysis system for reusable long-term 3D wound follow-up.

V. CONCLUSION

The main contribution of this study is to show that longitudinal wound measurement becomes more trustworthy when registration is anchored to stable anatomy rather than to the wound itself. We propose a longitudinal rigid-registration framework that excludes the dynamic wound region and uses only the peri-wound healthy-skin anchor to build spatial correspondences through a three-stage pipeline of PCA pre-alignment, RANSAC coarse registration, and ICP refinement. On the current dataset of four chronic-wound cases and seven longitudinal registration tasks, the method performs comparably to a robust baseline overall while showing failure-recovery capability on representative difficult cases. Under the resulting unified spatial reference, longitudinal quantification of area, volume, and depth captures wound-

healing and remodelling patterns more precisely than single-metric assessment.

More broadly, this work suggests that, in longitudinal lesion analysis, the choice of registration reference may matter more than incremental increases in algorithmic complexity. The spatial-weighting experiment further shows that explicitly encoding anatomical stability into ICP can reduce local error, although its benefit remains constrained by coarse-registration quality and anchor distribution. Larger cohorts, longer follow-up, and richer clinical outcome indicators are now needed to test the generalisability of this framework and to clarify its potential relation to tissue remodelling.

DATA AVAILABILITY STATEMENT

The data presented in this study are not publicly available due to privacy and ethical restrictions involving prospective clinical wound data. The data may be made available from the corresponding author (H.Y., imperman@imut.edu.cn) upon reasonable request and subject to approval by the Medical Ethics Committee of Inner Mongolia Baogang Hospital. The code used to support the findings of this study is available from the corresponding author upon reasonable request.

ACKNOWLEDGMENT

The authors thank the Department of Burn Surgery, Inner Mongolia Baogang Hospital, for providing clinical access and patient support during data acquisition. During the preparation of this manuscript, the authors used Gemini for English language polishing only. The authors reviewed and edited the output and take full responsibility for the content of this publication.

CONFLICTS OF INTEREST

The authors thank the Department of Burn Surgery, Inner Mongolia Baogang Hospital, for providing clinical access and patient support during data acquisition. During the preparation of this manuscript, the authors used Gemini for English language polishing only. The authors reviewed and edited the output and take full responsibility for the content of this publication.

AUTHOR CONTRIBUTIONS

Conceptualization, C.M. and H.Y.; methodology, C.M.; software, C.M.; validation, C.M.; formal analysis, C.M.; investigation, C.M.; resources, H.Y.; data curation, C.M.; writing–original draft preparation, C.M.; writing–review and editing, H.Y.; visualization, C.M.; supervision, H.Y.; project administration, H.Y.; funding acquisition, H.Y. (Author initials: C.M. = Chengtao Ma; H.Y. = Haidong Yang.) All authors have read and agreed to the published version of the manuscript.

FUNDING

This research was funded by the University-level Key Project of the 2026 College Students' Innovation and Entrepreneurship Training Program of Inner Mongolia University of Technology, grant number 2026020047.

INSTITUTIONAL REVIEW BOARD STATEMENT

The study was conducted in accordance with the Declaration of Helsinki (2013 revision), and approved by the Medical Ethics Committee of Inner Mongolia Baogang Hospital (protocol code 2026-MER-024, date of approval: 8 May 2026).

INFORMED CONSENT STATEMENT

Informed consent was obtained from all subjects involved in the study. Written informed consent has been obtained from the patients to publish this paper with anonymized wound images and 3D data.

REFERENCES

[1] C. K. Sen, "Human wound and its burden: Updated 2022 compendium of estimates," *Adv. Wound Care*, vol. 12, pp. 657–667, 2023, doi: 10.1089/wound.2023.0150.

[2] F. Diban, S. Di Lodovico, P. Di Fermo, et al., "Biofilms in chronic wound infections: Innovative antimicrobial approaches using the in vitro Lubbock chronic wound biofilm model," *Int. J. Mol. Sci.*, vol. 24, Art. no. 1004, 2023, doi: 10.3390/ijms24021004.

[3] M. C. Redmond, G. Gethin, and D. P. Finn, "A review of chronic wounds and their impact on negative affect, cognition, and quality of life," *Int. Wound J.*, vol. 22, Art. no. e70748, 2025, doi: 10.1111/iwj.70748.

[4] Y. J. Wu, L. P. Wu, and M. F. Yu, "The clinical value of intelligent wound measurement devices in patients with chronic wounds: A scoping review," *Int. Wound J.*, vol. 21, Art. no. e14843, 2024, doi: 10.1111/iwj.14843.

[5] M. C. Alonso, H. T. Mohammed, R. D. Fraser, et al., "Comparison of wound surface area measurements obtained using clinically validated artificial intelligence-based technology versus manual methods and the effect of measurement method on debridement code reimbursement cost," *Wounds*, vol. 35, pp. 387–394, 2023, doi: 10.25270/wnds/23031.

[6] C. L. Zhao, Y. C. Guo, L. L. Li, et al., "Non-invasive techniques for wound assessment: A comprehensive review," *Int. Wound J.*, vol. 21, Art. no. e70109, 2024, doi: 10.1111/iwj.70109.

[7] K. Moj, A. I., Z. K., et al., "3D measurement of chronic wounds in routine care: A review with practical guidance for smartphone photogrammetry," *Ann. Biomed. Eng.*, to be published, doi: 10.1007/s10439-026-04172-z.

[8] A. G. Cutti, M. G. Santi, A. H. Hansen, et al., "Accuracy, repeatability, and reproducibility of a hand-held structured-light 3D scanner across multi-site settings in lower limb prosthetics," *Sensors*, vol. 24, Art. no. 2350, 2024, doi: 10.3390/s24072350.

[9] D. Filko and E. K. Nyarko, "Autonomous robot-driven chronic wound 3D reconstruction and analysis system," *Robotics*, vol. 14, Art. no. 30, 2025, doi: 10.3390/robotics14030030.

[10] R. Bartl, T. Mocnik, G. Tinkhauser, et al., "A lightweight approach to 3D measurement of chronic wounds," *J. WSCG*, vol. 27, pp. 53–60, 2019, doi: 10.24132/jwscg.2019.27.1.8.

[11] P. Gholami, M. A. Ahmadi-Pajouh, N. Abolftahi, et al., "Segmentation and measurement of chronic wounds for bioprinting," *IEEE J. Biomed. Health Inform.*, vol. 22, no. 4, pp. 1269–1277, 2018, doi: 10.1109/JBHI.2017.2743526.

[12] H. Chi, M. Liu, J. Wang, et al., "Cross-hierarchical decoding with SAM for semi-supervised medical image segmentation," *IEEE Trans. Circuits Syst. Video Technol.*, vol. 36, pp. 3742–3753, 2026, doi: 10.1109/TCSVT.2025.3625276.

[13] H. Wang, S. Guo, J. Ye, et al., "SAM-Med3D: A vision foundation model for general-purpose segmentation on volumetric medical images," *IEEE Trans. Neural Netw. Learn. Syst.*, vol. 36, pp. 17599–17612, 2025, doi: 10.1109/TNNLS.2025.3586694.

[14] N. Curti, Y. Merli, C. Zengarini, et al., "Effectiveness of semi-supervised active learning in automated wound image segmentation," *Int. J. Mol. Sci.*, vol. 24, Art. no. 706, 2023, doi: 10.3390/ijms24010706.

[15] P. Zhang, Y. C. Zhang, and Q. Li, "RGB-D camera-based automatic wound-measurement system," *IEEE Trans. Instrum. Meas.*, vol. 72, pp. 1–11, 2023, doi: 10.1109/TIM.2023.3265758.

[16] D. Filko, R. Cupec, and E. K. Nyarko, "Wound measurement by RGB-D camera," *Mach. Vis. Appl.*, vol. 29, pp. 633–654, 2018, doi: 10.1007/s00138-018-0920-4.
[17] P. Sheehan, P. Jones, A. Caselli, et al., "Percent change in wound area of diabetic foot ulcers over a 4-week period is a robust predictor of complete healing in a 12-week prospective trial," *Diabetes Care*, vol. 26, no. 6, pp. 1879–1882, 2003, doi: 10.2337/diacare.26.6.1879.
[18] O. A. Pena and P. Martin, "Cellular and molecular mechanisms of skin wound healing," *Nat. Rev. Mol. Cell Biol.*, vol. 25, pp. 599–616, 2024, doi: 10.1038/s41580-024-00715-1.
[19] P. J. Besl and N. D. McKay, "A method for registration of 3-D shapes," *IEEE Trans. Pattern Anal. Mach. Intell.*, vol. 14, no. 2, pp. 239–256, 1992, doi: 10.1109/34.121791.
[20] Y. Chen and G. Medioni, "Object modelling by registration of multiple range images," *Image Vis. Comput.*, vol. 10, no. 3, pp. 145–155, 1992, doi: 10.1016/0262-8856(92)90066-C.
[21] M. A. Fischler and R. C. Bolles, "Random sample consensus: A paradigm for model fitting with applications to image analysis and automated cartography," *Commun. ACM*, vol. 24, no. 6, pp. 381–395, 1981, doi: 10.1145/358669.358692.
[22] R. B. Rusu, N. Blodow, and M. Beetz, "Fast Point Feature Histograms (FPFH) for 3D registration," in *Proc. IEEE Int. Conf. Robot. Autom. (ICRA)*, Kobe, Japan, May 2009, pp. 3212–3217, doi: 10.1109/ROBOT.2009.5152473.
[23] A. Myronenko and X. Song, "Point set registration: Coherent point drift," *IEEE Trans. Pattern Anal. Mach. Intell.*, vol. 32, no. 12, pp. 2262–2275, 2010, doi: 10.1109/TPAMI.2010.46.
[24] B. Jian and B. C. Vemuri, "Robust point set registration using Gaussian mixture models," *IEEE Trans. Pattern Anal. Mach. Intell.*, vol. 33, no. 8, pp. 1633–1645, 2011, doi: 10.1109/TPAMI.2010.223.
[25] Z. Yang, J. S. Heiselman, C. Han, et al., "Resolving the ambiguity of complete-to-partial point cloud registration for image-guided liver surgery with patches-to-partial matching," *IEEE J. Biomed. Health Inform.*, vol. 30, pp. 459–472, 2026, doi: 10.1109/JBHI.2025.3583875.
[26] J. P. Thirion, "Image matching as a diffusion process: An analogy with Maxwell's demons," *Med. Image Anal.*, vol. 2, no. 3, pp. 243–260, 1998, doi: 10.1016/S1361-8415(98)80022-4.
[27] B. B. Avants, C. L. Epstein, M. Grossman, et al., "Symmetric diffeomorphic image registration with cross-correlation: Evaluating automated labeling of elderly and neurodegenerative brain," *Med. Image Anal.*, vol. 12, no. 1, pp. 26–41, 2008, doi: 10.1016/j.media.2007.06.004.
[28] S. Klein, M. Staring, K. Murphy, et al., "elastix: A toolbox for intensity-based medical image registration," *IEEE Trans. Med. Imaging*, vol. 29, no. 1, pp. 196–205, 2010, doi: 10.1109/TMI.2009.2035616.
[29] B. B. Avants, N. J. Tustison, G. Song, et al., "A reproducible evaluation of ANTs similarity metric performance in brain image registration," *NeuroImage*, vol. 54, no. 3, pp. 2033–2044, 2011, doi: 10.1016/j.neuroimage.2010.09.025.
[30] G. Balakrishnan, A. Zhao, M. R. Sabuncu, et al., "VoxelMorph: A learning framework for deformable medical image registration," *IEEE Trans. Med. Imaging*, vol. 38, no. 8, pp. 1788–1800, 2019, doi: 10.1109/TMI.2019.2897538.
[31] M. Reuter, N. J. Schmansky, H. D. Rosas, et al., "Within-subject template estimation for unbiased longitudinal image analysis," *NeuroImage*, vol. 61, no. 4, pp. 1402–1418, 2012, doi: 10.1016/j.neuroimage.2012.02.084.
[32] I. Csapo, B. Davis, Y. Shi, et al., "Longitudinal image registration with non-uniform appearance change," in *Proc. Med. Image Comput. Comput.-Assist. Interv. (MICCAI)*, Nice, France, 2012, pp. 280–288, doi: 10.1007/978-3-642-33454-2_35.
[33] I. Csapo, B. Davis, Y. Shi, et al., "Longitudinal image registration with non-uniform appearance change," *Med. Image Comput. Comput.-Assist. Interv.*, pp. 280–288, 2012, doi: 10.1007/978-3-642-33454-2_35.
[34] X. Li, L. R. Arlinghaus, A. B. Chakravarthy, et al., "Early DCE-MRI changes after longitudinal registration may predict breast cancer response to neoadjuvant chemotherapy," in *Proc. Biomed. Image Registration*, Nashville, TN, USA, 2012, pp. 229–235, doi: 10.1007/978-3-642-31340-0_24.
[35] C. Mattusch, U. Bick, F. Michallek, et al., "Development and validation of a four-dimensional registration technique for DCE breast MRI," *Insights Imaging*, vol. 14, Art. no. 17, 2023, doi: 10.1186/s13244-022-01362-w.